# Hydrogen Peroxide Photolysis in Acidic Aqueous Solutions Containing Chloride Ions. II. Quantum Yield of HO•(Aq) Radicals

**Xiao-Ying Yu[†,‡] and John R. Barker*[,†,§]**

*Department of Chemistry, The University of Michigan, Ann Arbor, Michigan 48109-1055, and Department of Atmospheric, Oceanic, and Space Sciences, The University of Michigan, Ann Arbor, Michigan 48109-2143*

*Received: August 1, 2002; In Final Form: November 19, 2002*

Chloride ion is used as an efficient scavenger of hydroxyl radicals to measure the yield of HO• produced in the photolysis of acidic aqueous solutions of hydrogen peroxide. The scavenging efficiency is shown to depend on the chloride ion concentration and solution acidity, as expected from the mechanism. The results show that the quantum yield of hydroxyl radicals produced from hydrogen peroxide photodissociation in the aqueous phase is close to unity at both 248 and 308 nm: $\Phi_{HO\cdot}(248\text{ nm}) = 1.0 \pm 0.1$ and $\Phi_{HO\cdot}(308\text{ nm}) = 0.8 \pm 0.2$, where the uncertainties ($\pm\sigma$) were obtained from propagation of errors. [Because of geminate recombination in the solvent cage, quantum yields in solution are often smaller than those in the gas phase, where the HO• quantum yields are equal to 2.] The present results for the aqueous phase are generally consistent with other determinations.

## Introduction

Hydroxyl radicals play a cardinal role in tropospheric chemistry.[1] Aqueous phase hydroxyl radicals HO•(aq) are very strong oxidants, and their reactions are important in the chemical transformations of atmospheric species. A well-known example is the free radical oxidation of S(IV) to S(VI).[2] Photolysis of hydrogen peroxide is one of the main sources of hydroxyl radicals in atmospheric liquid water:[3−7]

$$H_2O_{2(aq)} + h\nu \rightarrow HO^{\bullet}_{(aq)} + HO^{\bullet}_{(aq)} \qquad (1)$$

Knowledge of the primary quantum yield for the production of hydroxyl radicals by hydrogen peroxide photodissociation is important for accurate descriptions of the atmospheric aqueous phase.

The primary quantum yield of hydroxyl radicals by photodissociation of hydrogen peroxide is defined as follows:

$$\Phi_{HO\cdot} = [HO^{\bullet}]_0/[h\nu]_\lambda \qquad (I)$$

where $[HO^{\bullet}]_0$ is the initial concentration of thermalized hydroxyl radicals produced by $H_2O_2$ photolysis and $[h\nu]_\lambda$ is the concentration of photons absorbed by $H_2O_2$ at the photolysis wavelength $\lambda$.

In the gas phase, $\Phi_{HO\cdot} = 2$ because two hydroxyl radicals are produced by breaking the O−O bond in each hydrogen peroxide molecule that absorbs a photon. However, $\Phi_{HO\cdot}$ in solution is often significantly lower than in the gas phase, because free radicals can recombine or form other species before escaping the solvent cage.[8] The primary quantum yield of hydroxyl radicals ($\Phi_{HO\cdot}$) is twice the magnitude of the primary quantum yield of hydrogen peroxide photodissociation ($\Phi_{H_2O_2}$) because two HO• radicals are produced for each $H_2O_2$ that dissociates. However, the total quantum yield of $H_2O_2$ destruction ($\Phi_D$) does not equal $\Phi_{H_2O_2}$, because secondary reactions affect the magnitude of $\Phi_D$. Several groups have measured $\Phi_D$ in the aqueous phase under conditions where free radical chain reactions were important.[9−18] Discrepancies exist among those results because the chain lengths differed in different experiments.

In the present work, the scavenger method is used to determine $[HO^{\bullet}]_0$.[19] The scavenger method is widely used in kinetic studies when direct observation of a chemical species is difficult. In this case, hydroxyl radicals absorb light relatively weakly and hence are difficult to measure. However, reaction of HO• with a suitable scavenger can produce a product species that absorbs strongly and is easy to measure. Halide ions ($X^- = Cl^-$, $Br^-$, etc.) and pseudo-halide ions ($X^- = SCN^-$, etc.) are good scavengers for the determination of HO• radicals, because they react with HO• rapidly and the strongly absorbing transient free radical species $X_2^{-\bullet}$ is formed after a few rapid reaction steps. Other scavengers have also been used in the determination of $\Phi_{HO\cdot}$. For example, Hatada et al. employed *p*-nitrosodimethylaniline.[20]

In the present work, chloride ion ($Cl^-$) is used as the scavenger. As explained below, experimental complications[21−23] that attend photolysis at 248 nm preclude the use of thiocyanate ($SCN^-$), which is a more common choice.[24,25] The choice of chloride ion is particularly appropriate because the detailed mechanism involving chloride ions and hydroxyl radicals has been investigated in our laboratory and is being reported in a series of papers. Paper I describes the chemical mechanism and presents several new measurements of rate constants and equilibrium constants.[26] The present paper is designated Paper II. Paper III presents new results obtained using photolysis of $K_2S_2O_8$ to produce sulfate radicals ($SO_4^{-\bullet}$), which initiated free radical reactions involving $Cl^-$, Cl•(aq), and $Cl_2^{-\bullet}$.[27] In Paper IV, several important rate constants are critically evaluated.[28]

Chloride ions are abundant in seawater, sea salt aerosols, cloudwater and rain droplets. Hydroxyl radicals react very

* To whom correspondence should be addressed. E-mail: jrbarker@umich.edu.

† Department of Chemistry, The University of Michigan.

‡ Present Address: Department of Atmospheric Science, Colorado State University, Fort Collins, Colorado 80523-1371.

§ Department of Atmospheric, Oceanic, and Space Sciences, The University of Michigan.

10.1021/jp026666s CCC: $25.00 
Published on Web 02/07/2003

**TABLE 1: Reaction Mechanism with Recommended Rate Constants, $k_i$, and Equilibrium Constants, $K_i$ (see Paper I)**

| | reaction | $k_f$ | $k_r$ |
|---|---|---|---|
| 1 | $H_2O_2 + h\nu \rightarrow HO^\bullet + HO^\bullet$ | $\phi_{OH} = 1$ [a] | |
| 2 | $HO^\bullet + H_2O_2 \rightarrow HO_2 + H_2O$ | $k_2 = (4.2 \pm 0.2) \times 10^7$ $M^{-1}s^{-1}$ [b] | |
| 3 | $HO^\bullet + Cl^- \leftrightarrow ClOH^{-\bullet}$ | $k_3 = (4.3 \pm 0.4) \times 10^9$ $M^{-1}s^{-1}$ [30] | $k_{-3} = (6.1 \pm 0.8) \times 10^9$ $M^{-1}s^{-1}$ [30] |
| | | $K_3 = 0.70 \pm 0.13$ $M^{-1}$ [30] | |
| 4 | $ClOH^{-\bullet} + H^+ \leftrightarrow Cl^\bullet + H_2O$ | $k_4 = (2.6 \pm 0.6) \times 10^{10}$ $M^{-1}s^{-1}$ [b] | $k_{-4} = (3.6 \pm 0.4) \times 10^3$ $M^{-1}s^{-1}$ [b,c] |
| | | $k_4^\circ = (3.2 \pm 0.7) \times 10^{10}$ $M^{-1}s^{-1}$ [b] | |
| | | $K_4 = (7.2 \pm 1.6) \times 10^6$ [b] | |
| | | $K_4^0 = (8.8 \pm 2.2) \times 10^6$ [b] | |
| 5 | $Cl^\bullet + Cl^- \leftrightarrow Cl_2^{-\bullet}$ | $k_5 = (7.8 \pm 0.8) \times 10^9$ $M^{-1}s^{-1}$ [c] | $k_{-5} = (5.2 \pm 0.3) \times 10^4$ $s^{-1}$ [b] |
| | | | $k_{-5} = (5.7 \pm 0.3) \times 10^4$ $s^{-1}$ [c] |
| | | $K_5 = (1.4 \pm 0.2) \times 10^5$ $M^{-1}$ [b,c] | |
| 6 | $Cl_2^{-\bullet} + Cl_2^{-\bullet} \rightarrow 2Cl^- + Cl_2$ | $k_6 = (9 \pm 1) \times 10^8$ $M^{-1}s^{-1}$ [b] | |
| | | $k_6^\circ = (7.2 \pm 0.8) \times 10^8$ $M^{-1}s^{-1}$ [b] | |
| 7 | $Cl^\bullet + Cl_2^{-\bullet} \rightarrow Cl^- + Cl_2$ | $k_7 = (2.1 \pm 0.05) \times 10^9$ $M^{-1}s^{-1}$ [d] | |
| 8 | $Cl_2^{-\bullet} + H_2O \rightarrow ClOH^{-\bullet} + H^+ + Cl^-$ | $k_8[H_2O] < 100$ $s^{-1}$ [b] | |
| 9 | $Cl_2^{-\bullet} + H_2O_2 \rightarrow HO_2^\bullet + H^+ + 2\,Cl^-$ | $k_9 = (1.4 \pm 0.2) \times 10^6$ $M^{-1}s^{-1}$ [b] | |
| 10 | $Cl^\bullet + H_2O_2 \rightarrow H^+ + Cl^- + HO_2^\bullet$ | $k_{10} = (2.0 \pm 0.3) \times 10^9$ $M^{-1}s^{-1}$ [b] | |
| 11 | $Cl_2^{-\bullet} + HO_2^\bullet \rightarrow O_2 + H^+ + 2\,Cl^-$ | $k_{11} = (3.1 \pm 1.5) \times 10^9$ $M^{-1}s^{-1}$ [e] | |
| 12 | $HO_2^\bullet + H_2O_2 \rightarrow H_2O + O_2 + HO^\bullet$ | $k_{12} = 0.5$ $M^{-1}s^{-1}$ [54] | |
| 13 | $HO^\bullet + HO^\bullet \rightarrow H_2O_2$ | $k_{13} = 6.0 \times 10^9$ $M^{-1}s^{-1}$ [55] | |
| 14 | $HO^\bullet + HO^\bullet \rightarrow H_2O + O^\bullet$ | - - - - | |
| 15 | $HO_2^\bullet + HO_2^\bullet \rightarrow H_2O_2 + O_2$ | $k_{15} = 9.8 \times 10^5$ $M^{-1}s^{-1}$ [56] | |
| 16 | $HO^\bullet + HO_2^\bullet \rightarrow H_2O + O_2$ | $k_{16} = 1.0 \times 10^{10}$ $M^{-1}s^{-1}$ [57] | |

[a] This work. [b] Paper I, uncertainties ($\pm 1\sigma$) were obtained from error propagation; ionic strength $\mu \approx 0.01$ M unless otherwise noted by a superscript "0" on rate or equilibrium constants that have been adjusted to $\mu = 0$.[26] [c] Literature evaluation (Paper I), uncertainties ($\pm 1\sigma$) obtained from error propagation.[26] [d] See Paper III.[27] [e] See Paper IV.[28]

rapidly with chloride ions to form $ClOH^{-\bullet}$, which can react with $H^+$ to produce $Cl^\bullet$.[26,29,30] Subsequent reaction produces the dichloride radical anion, $Cl_2^{-\bullet}$, which can be monitored by UV absorption spectroscopy. The yield of $Cl_2^{-\bullet}$ depends on both the scavenger concentration and the solution acidity, as demonstrated in this paper. Quantitative scavenging of $HO^\bullet$ to produce measured $Cl_2^{-\bullet}$ allows quantitative determination of $[HO^\bullet]_0$.

### Scavenger Method for Determination of $[HO\bullet]_0$

A suitable scavenger will react with hydroxyl radicals faster than competing reactions. Ideally, photolysis of the scavenger in the absence of $HO^\bullet$ radicals should not generate detectable products. Furthermore, the chemical mechanism should be known in sufficient detail so that $[HO^\bullet]_0$ can be obtained with confidence.

The thiocyanate ion, $SCN^-$, has been used to measure $\Phi_{HO^\bullet}$ from photolysis of $H_2O_2$ at 308 and 351 nm.[24] However, we found that photolysis of $SCN^-$ at 248 nm generates $(SCN)_2^{-\bullet}$, causing significant interference. The decomposition products of $(SCN)_2^{-\bullet}$ were found to form tiny suspended particles that attenuate light in the wavelength range from 180 to 650 nm. We visually observed strong emission in the red part of the spectrum during photolysis of thiocyanate ions. In addition, the formation of a white precipitate was observed if the photolyzed solution was allowed to stand after photolysis. Previously, Jablczynski and Jablczyska[21] concluded that the photodissociation of $SCN^-$ should produce sulfur and Matheson et al.[22] reported the observation of red emission after photolysis of $SCN^-$, which is identical to what was seen in our experiments. Similarly, Dogliotti and Hayon[23] observed light attenuation by the formation of elemental sulfur in the wavelength range of 180 to 650 nm. We surmise that the particles in our experiments consist of elemental sulfur and may also emit light in that same range.

Because of these serious interferences, we investigated chloride ions, bromide ions, and iodide ions as potential scavengers for $HO^\bullet$ produced by 248 nm photolysis of $H_2O_2$. The photolysis of iodide ions in the absence of $H_2O_2$ produces

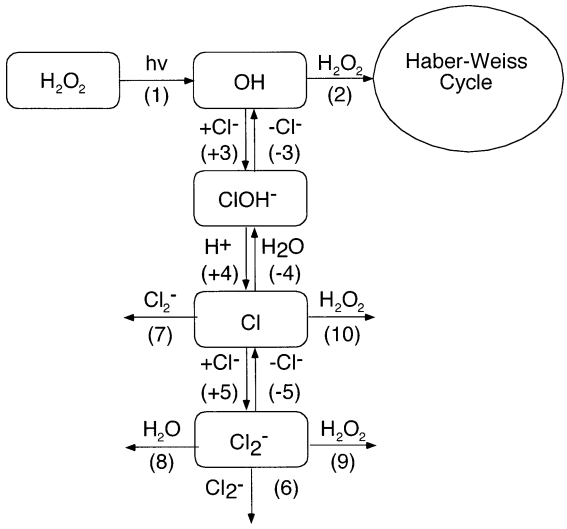


**Figure 1.** Reaction Mechanism Flow Chart. Reaction numbers (Table 1) are shown in parentheses.

several transient species[19] that undergo complicated sequential reactions. Furthermore, the $I_x^{-\bullet}$ ($x = 2$, 3, 4, 5, and 6) species all absorb light strongly, leading to potential interferences. Because of all of these complications, we rejected $I^-$ as a scavenger. Both bromide ions and chloride ions appeared to behave in a "clean" fashion and are therefore possible choices of hydroxyl radical scavenger. Because we have been investigating the chemical mechanism involving $Cl^-$, we selected chloride ions as the scavenger in the present work. Photolysis of $Cl^-$ at 248 and 308 nm in the absence of $H_2O_2$ does not produce detectable amounts of $Cl_2^{-\bullet}$. In addition, subsequent reaction products do not interfere with the detection of $Cl_2^{-\bullet}$, which is produced very rapidly under acidic conditions.

When $Cl^-$ is used as a scavenger, three steps are needed to produce $Cl_2^{-\bullet}$, which then decays via several routes (see Table 1 and Figure 1). These reactions compete with reaction 2, in which $HO^\bullet$ attacks $H_2O_2$, resulting in a free radical chain reaction that destroys $H_2O_2$ (the Haber−Weiss cycle[31−33]). The quantita-

tive scavenging of hydroxyl radicals to form $Cl_2^{-\bullet}$ depends on the concentration of $Cl^-$ relative to that of $H_2O_2$ and on the acidity of the solution, i.e., $[H^+]$. When reactions that are second order in radical concentration can be neglected, the essential features of the reaction mechanism can be summarized with only a few steps (see Table 1 for reaction numbering):

$$H_2O_2 + h\nu \rightarrow HO^\bullet + HO^\bullet \quad (1)$$

$$HO^\bullet + H_2O_2 \rightarrow HO_2\cdot + H_2O \quad (2)$$

$$HO^\bullet + Cl^- + (H^+) \rightarrow Cl^\bullet + H_2O \quad (g)$$

$$Cl^\bullet + Cl^- \rightarrow Cl_2^{-\bullet} \quad (5,-5)$$

$$Cl^\bullet + H_2O_2 \rightarrow H^+ + Cl^- + HO_2\cdot \quad (10)$$

In this reduced mechanism, reaction g is the result of combining reactions 3, −3, and 4 via the pseudo-steady-state approximation for $[ClOH^{-\bullet}]$:[26]

$$k_g = \frac{k_3 k_4 [H^+]}{k_{-3} + k_4 [H^+]} = k_g'[H^+] \quad (II)$$

When $k_{-3} \gg k_4[H^+]$, eq II reduces to $k_g \approx k_g'[H^+] = K_3 k_4 [H^+]$, where $K_3$ is the equilibrium constant for reaction 3 [notation: equilibrium constants upper case, rate constants lower case].

Under the assumption that there is no loss of $Cl_2^{-\bullet}$ on the time scale of the experiments and assuming that all of the $HO^\bullet$ radicals react with chloride ions, the yield of $Cl_2^{-\bullet}$ can be identified with $[HO^\bullet]_0$, the primary yield of $HO^\bullet$ radicals in photolysis of $H_2O_2$. When $HO^\bullet$ radicals can also react significantly with other species, then a correction is necessary. In the experiments, $[Cl_2^{-\bullet}]$ rises very rapidly to a maximum and then decays slowly. The slow decay is extrapolated back to $t = 0$ to obtain $[Cl_2^{-\bullet}]_0$, the apparent initial concentration of $Cl_2^{-\bullet}$ (see below). If the loss of $[Cl_2^{-\bullet}]$ is small, as in the present work, then the short extrapolation back to $t = 0$ can be carried out equally well by assuming the rate of loss is either first order or second order in $[Cl_2^{-\bullet}]$.

Because $HO^\bullet$ radicals can react with both $Cl^-$ and $H_2O_2$, a correction is needed in order to relate the measured value of $[Cl_2^{-\bullet}]_0$ to $[HO^\bullet]_0$. The reaction of $[HO^\bullet]$ is assumed to take place under pseudo-first-order conditions with rate constant $k_A = k_2[H_2O_2] + k_g[Cl^-]$. By assuming pseudo-steady-state for $[ClOH^{-\bullet}]$ and for $[Cl^\bullet]$, the following expression for $[Cl_2^{-\bullet}]$ is obtained:

$$[Cl_2^{-\bullet}] = Q\{e^{-k_A t} - e^{-k_C t}\} \quad (IIIa)$$

where

$$k_A = k_2[H_2O_2] + k_g[Cl^-] \quad (IIIb)$$

$$k_C = \frac{k_{-5} k_{10} [H_2O_2]}{k_5[Cl^-] + k_{10}[H_2O_2]} \quad (IIIc)$$

$$Q = \frac{[HO^\bullet]_0}{\left[\frac{1}{K_5[Cl^-]}\frac{k_{10}[H_2O_2]}{k_g[Cl^-]}\right] - \left[1 + \frac{k_{10}[H_2O_2]}{k_5[Cl^-]}\right]\left[1 + \frac{k_2[H_2O_2]}{k_g[Cl^-]}\right]} \quad (IIId)$$

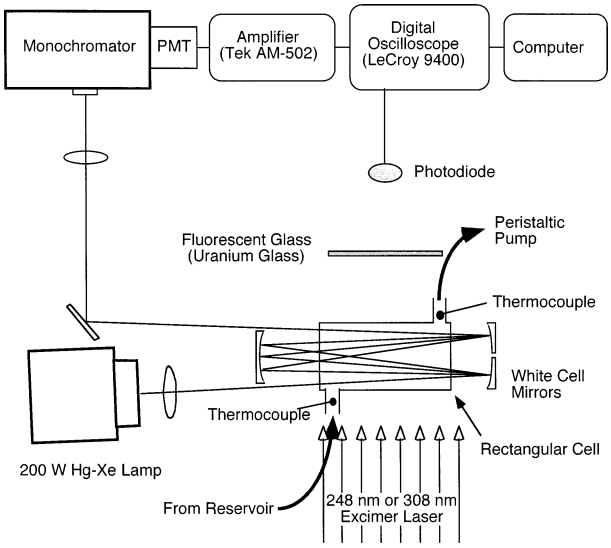


**Figure 2.** Schematic diagram of the experimental apparatus.

Note that the *sign* of $Q$ is perfectly correlated with the *sign* of the factor in curly brackets in eq IIIa: $[Cl_2^{-\bullet}]$ is always positive, but the quantity $Q$ can be either positive or negative.

When the magnitudes of $k_A$ and $k_C$ are significantly different from one another, $[Cl_2^{-\bullet}]$ increases rapidly and decays slowly. When the rise time is short relative to the decay time, then $Q$ is positive and the short extrapolation gives a value at $t = 0$ that is essentially indistinguishable from $Q$. There are two limiting cases for $Q$, corresponding to the cases when $k_A \gg k_C$ and vice versa:

$$Q = \frac{[HO^\bullet]_0}{\left[1 + \frac{k_{10}[H_2O_2]}{k_5[Cl^-]}\right]\left[1 + \frac{k_2[H_2O_2]}{k_g[Cl^-]}\right]} \quad (IVa)$$

$$Q = \frac{[HO^\bullet]_0 K_5 k_g [Cl^-]^2}{k_{10}[H_2O_2]} \quad (IVb)$$

In our data analysis, we equate the two quantities, $Q = [Cl_2^{-\bullet}]_0$, because the rise time is much shorter than the decay time. Under all of the experimental conditions employed in the present work, $k_A \gg k_C$ and $[Cl_2^{-\bullet}]_0$ is described approximately by eq IVa. Scavenging is essentially complete when $k_g$ is large (low pH) and $k_5[Cl^-] \gg k_{10}[H_2O_2]$. Under intermediate conditions, scavenging is less efficient and it is possible to determine the rate constant ratios that appear in the denominator of eq IVa. However, the neglected reactions that are second order in free radical concentration may be more important under intermediate conditions, making eq IVa less accurate.

## Experimental Section

**Apparatus.** A schematic diagram of the experimental apparatus is shown in Figure 2. The photolysis source is a Lambda Physik Excimer Multi-gas Laser (EMG 101) operating at 248 (KrF) and 308 nm (XeCl). The laser pulse energy was 40∼65 J $m^{-2}$ at 248 nm and 30∼40 J $m^{-2}$ at 308 nm. The pulse half-width is ∼15 ns, and the beam cross sectional area is 10 $cm^2$ defined by an aperture of 25 × 40 mm. The laser beam traverses ∼4−5 m before reaching the cell. A rectangular mask is used so that only the central uniform portion of the beam is allowed to enter the cell. The reactant solutions are irradiated in a quartz

cell of external dimensions 25 × 25 × 47 mm. The temperatures of the liquid entering and leaving the cell are measured by copper−constantan thermocouples supported in borosilicate glass thermocouple wells at the entrance and exit of the cell. The temperature was 297 ± 2 K in all experiments described here. All connections are made using Teflon tubing and connectors, so that the solutions come into contact only with borosilicate glass, fused silica, and Teflon.

The experiments were carried out in a manner that used the solutions economically but did not sacrifice accuracy. By direct tests, it was found that the laser pulse repetition rate could be varied from 0.3 to 10 Hz and the volume flow rate could be varied from 1 to 10 mL $s^{-1}$ without affecting the measured rate parameters. In most experiments, the laser pulse repetition rate was held at 1.0 Hz by a digital delay/pulse generator (Stanford Research Systems, model DG535), and the flow of the solutions through the cell was controlled at 2.2 $cm^3$ $s^{-1}$ by a peristaltic pump (Masterflex model 7553-70). At this flow rate, cavitation of the solution did not occur.

A high-pressure xenon mercury arc lamp (200W, Oriel model 6291) with a regulated power supply (Oriel 68805 Universal Power Supply, 40-200W) provided a continuous light source for monitoring transient species. White cell optics were utilized to fold the optical path in the cell in order to enhance detection sensitivity.[34] The typical number of paths ranged from 4 to 16, i.e., path lengths from 16 to 64 cm. A Jarrell-Ash Monochromator (model 82-410) and a Hamamatsu 1P28 photomultiplier (with Hamamatsu E717−05 socket) were used to monitor the transmitted light. An anode load resistor of 1200 Ω produced a voltage signal with a measured instrument time constant on the order of 1 μs and limited the photomultiplier anode current to ≤4 μA, ensuring photomultiplier linearity. The voltage signal from the anode resistor was amplified with a Tektronix AM 502 differential amplifier and then sent through an over-voltage protector (Huber & Suhnerm 3401.01. G, 50 Ω, 230 V) to a LeCroy 9400 oscilloscope, which was triggered by the laser pulse as viewed using a silicon photodiode. Typically, 200−250 laser shots were averaged to obtain each experimental trace. The averaged data were transferred to a Macintosh computer for subsequent analysis. Least-squares fits of the experimental data were carried out using KaleidaGraph plotting software (Synergy Software), which utilizes the Levenberg−Marquardt nonlinear least squares algorithm.[35] When weighted data analysis was performed, weighting was based on the error of each data point.

The absorption due to $HO^•$ is very small compared to that due to $Cl_2^{-•}$.[36,37] We monitored $Cl_2^{-•}$ by its absorption at 364 nm ($\epsilon_{Cl_2^{-•},364\ nm}$ = 7000 ± 700 $M^{-1}$ $cm^{-1}$),[27] which is the wavelength of the strongest output band of the xenon−mercury lamp in the vicinity of the $Cl_2^{-•}$ absorption maximum (∼340 nm). [All absorption coefficients in this paper are base 10.] The strong emission gives better signal-to-noise ratios. This value for the extinction coefficient of $Cl_2^{-•}$ was determined[27] by the photolysis of solutions containing $SO_4^{-•}$ and $Cl^-$ using the same experimental setup as described here (see Paper 3[27] for details). The basic approach was to compare the absorptions due to $SO_4^{-•}$ and to $Cl_2^{-•}$, where the extinction coefficient employed for $SO_4^{-•}$ was the same as that measured recently by Buxton et al.[38] The resulting extinction coefficient for $Cl_2^{-•}$ given above is within 15% of most of the previous values at the wavelength of maximum absorption (see Paper 3[27] for details and for an error analysis). The spectra of $Cl^•$ and of $Cl_2^{-•}$ overlap around the detection wavelength.[37] The contribution of $Cl^•$ to the total absorption depends on [$Cl^-$] and the equilibrium constant of reaction 5. For the concentrations of $Cl^-$ in the present experiments, the absorption due to $Cl^•$ can be neglected because it is estimated to be less than 0.01% [($\epsilon_{Cl^•,340\ nm}$ = 3800 $M^{-1}$ $cm^{-1}$)[39] and ($\epsilon_{Cl_2^{-•},340\ nm}$ = 8500 ± 500 $M^{-1}$ $cm^{-1}$)[27]]. Although the transient species $ClOH^{-•}$ has been reported to absorb in the same spectral region as $Cl_2^{-•}$,[30] its contribution to the total absorption signal is negligible under acidic conditions because its concentration is very low.

**Reagents.** All reagents used were of ACS grade. Sodium chloride (99.999%) and sodium perchlorate (98∼102%) anhydrous were purchased from Alfa *Æ*SR. Perchloric acid (70% $HClO_4$) was from Aldrich. Potassium persulfate (≥99.0% $K_2S_2O_8$) and hydrogen peroxide (30% $H_2O_2$, inhibitor-free) were from Fisher. Hydrogen peroxide (30%) with stabilizer was from Aldrich. *All the data presented in this paper were obtained using stabilizer-free hydrogen peroxide to avoid the potential interferences due to the stabilizer.* Hydrogen peroxide with stabilizer was used for only a few tests to determine whether the stabilizer would make any difference in our results.

All solutions were prepared immediately before experiments. The pH (0∼4) of all solutions was adjusted by adding perchloric acid ($HClO_4$). The pH of each solution was measured by a digital ionalyzer (Orion Research 501) equipped with a glass pH electrode calibrated with buffer solutions purchased from Fisher. Water was purified by a Milli-RO and Milli-Q system (resistivity ≥18 MΩ cm). Concentrations of hydrogen peroxide were determined by the Iodine Method[40] and were repeated daily. The concentration of $H_2O_2$ was usually ∼$10^{-4}$ and ∼$10^{-2}$ M for experiments carried out at 248 and 308 nm, respectively. The concentrations of NaCl ranged from 5 × $10^{-6}$ to ∼1 M.

Dissolved air was contained in the solutions. In some experiments, the dissolved air was removed by purging with argon gas (99.999%, Liquid Carbonic Corporation), but we found that the presence of dissolved air does not affect the results, in agreement with the reaction mechanism (see Table 1).

**Laser Pulse Energy.** To accommodate the large laser beam cross section, a 2 in. × 2 in. square uranium glass plate was used as the active element of a home-built energy meter. Light from the pulsed excimer laser struck the uranium glass and induced a pulse of strong yellow-green phosphorescence. A high-speed photodiode detector (Thorlabs Inc. DET2-S1) monitored the intensity of this induced phosphorescence, and the electronic signal was sent to a LeCroy 9400 oscilloscope. The phosphorescence light intensity was related to the laser pulse energy by comparison with measurements obtained using a calibrated volume absorbing calorimeter power meter (Scientech model 365). The plate-detector combination was held in a fixed geometry on a rotary pole. When the uranium glass plate and photodiode were rotated together (on the rotary pole) out of the laser beam, the power meter received the transmitted laser irradiation and gave a direct power reading of laser energy. For calibration purposes, the size of the laser beam was confined with apertures not exceeding the size of the power meter entrance, so that direct readings by the power meter could be compared with the phosphorescence intensity. The relationship between the direct power readings and the induced phosphorescence intensities was found to be nearly linear. The calibration was repeated daily. We estimate the relative errors associated with the laser pulse energy measurements are <5%.

Experiments were also carried out to determine the fraction of laser light reflected by each cell wall. This was accomplished by using pairs of photodiodes to measure the incident and reflected light intensities. As described elsewhere in detail,[41]

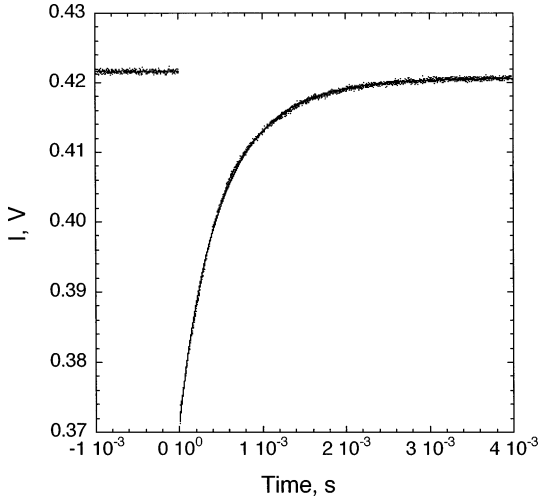


**Figure 3.** Typical time profile of $Cl_2^{-\bullet}$ absorption monitored at 364 nm. Experimental conditions: [NaCl] = 0.2 M, $[H_2O_2] = 5.22 \times 10^{-4}$ M, pH = 1.87. The solid line is generated by nonlinear least-squares analysis. The light intensity (*I*) is directly proportional to the voltage (*V*, after amplification) from a photodiode.

the intensity inside the cell was calculated using the measured values of the reflection coefficients and accounting for internal reflection inside the cell to obtain $f \approx 0.06$, the fraction of incident laser light reflected by each cell surface.

It is convenient to define the laser fluence: $F_\lambda = P/A$, where $P$ is the laser pulse energy transmitted by the cell and $A$ is the cross sectional area of the laser beam ($A \approx 10$ cm$^2$ in most experiments). Using these quantities, the concentration of laser photons absorbed by $H_2O_2$ in the cell is given by the following expression:

$$[h\nu]_\lambda = \frac{F_\lambda \ln(10)\, \epsilon_p\, [H_2O_2]_0}{N_A h\nu (1-f)^2} \qquad \text{(V)}$$

where $\epsilon_p$ is the absorption coefficient (base 10) of hydrogen peroxide at the laser wavelength, $N_A$ is Avogadro's number, $h\nu$ is the photon energy at the photolyzing wavelength, and $f$ is the reflection coefficient of the laser light reflected by the wall of the reaction cell. The extinction coefficients of hydrogen peroxide are 25 $M^{-1}cm^{-1}$ at 248 nm[42,43] and 1 $M^{-1}$ $cm^{-1}$ at 308 nm.[44]

## Results and Discussion

A typical time profile of the transient light absorption by $Cl_2^{-\bullet}$ monitored at 364 nm is shown in Figure 3. The solid line is a least-squares fit for mixed-first-and-second-order decay kinetics.[45,46] The signal prior to $t = 0$ corresponds to the initial intensity ($I_0$) of the monitoring light beam. The transient absorption causes the sharp decrease in transmitted intensity ($I_t$), which slowly recovers at later times. The absorbance at any time can be calculated according to Beer−Lambert law: $A_t = \log_{10}(I_0/I_t)$, where the time-dependent absorbance is proportional to the optical path length $s$ of the monitoring light, the absorption coefficient $\epsilon_{Cl_2^{-\bullet}}$, and the time-dependent concentration of $Cl_2^{-\bullet}$: $A_t = \epsilon_{Cl_2^{-\bullet}} s [Cl_2^{-\bullet}]_t$. Experimental runs were repeated in all cases to determine the run-to-run repeatability. For the present experiments, $A_t$ was extrapolated back to $t = 0$ in order to determine the initial yield of $Cl_2^{-\bullet}$ resulting from the laser pulse.

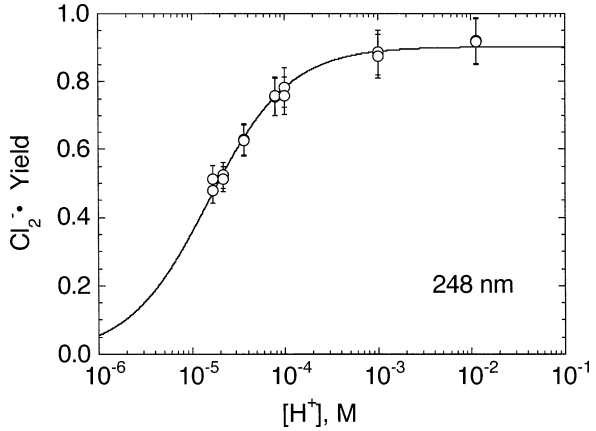


**Figure 4.** Dependence of $Cl_2^{-\bullet}$ yield (248 nm) on $[H^+]$ at $[Cl^-] = 0.2$ M and $[H_2O_2] = 5.345 \times 10^{-4}$ M. The solid line is nonlinear least-squares fit to eq VII.

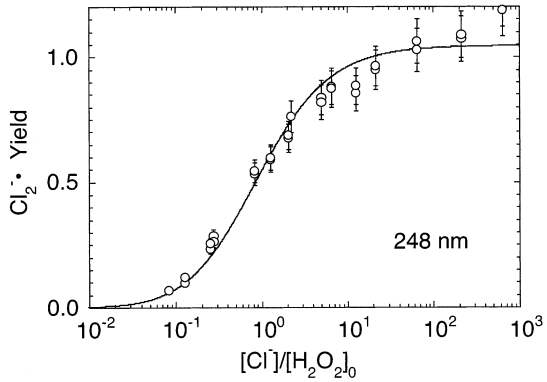


**Figure 5.** Dependence of $Cl_2^{-\bullet}$ yield (248 nm) on $[Cl^-]/[H_2O_2]$ at pH = 1. The solid line is nonlinear least-squares fit to eq VII.

The following expression is obtained from eqs IVa and V:

$$\frac{[Cl_2^{-\bullet}]_0}{F_\lambda [H_2O_2]_0} = \frac{\ln(10)\, \epsilon_p}{N_A h\nu (1-f)^2} \frac{\Phi_{HO\bullet}}{\left[1 + \frac{k_{10}[H_2O_2]}{k_5[Cl^-]}\right]\left[1 + \frac{k_2[H_2O_2]}{k_g[Cl^-]}\right]} \qquad \text{(VI)}$$

By rearranging eq VI, one obtains an expression in which the left-hand side is the experimental yield of $Cl_2^{-\bullet}$, Yield, and the right-hand side is proportional to $\Phi_{HO\bullet}$:

$$\text{Yield} = \frac{A_0}{F_\lambda [H_2O_2]_0} \cdot \frac{N_A h\nu (1-f)^2}{s\epsilon_{Cl_2^{-\bullet}} \ln(10)\, \epsilon_p} = \frac{\Phi_{HO\bullet}}{\left[1 + \frac{k_{10}[H_2O_2]}{k_5[Cl^-]}\right]\left[1 + \frac{k_2[H_2O_2]}{k_g[Cl^-]}\right]} \qquad \text{(VII)}$$

where $[Cl_2^{-\bullet}]_0$ is expressed in terms of the measured initial absorbance ($A_0$, base 10), $\epsilon_{Cl_2^{-\bullet}} = 7000$ $M^{-1}$ $cm^{-1}$ is the absorption coefficient[27] of $Cl_2^{-\bullet}$ at the monitoring wavelength of 364 nm, and $k_g'[H^+] = k_g$ (see eq II).

The Yield of $Cl_2^{-\bullet}$ measured at 248 nm with $[Cl^-] = 0.2$ M and $[H_2O_2] = 5.345 \times 10^{-4}$ M is plotted vs $[H^+]$ in Figure 4 and vs $[Cl^-]/[H_2O_2]$ for pH = 1 in Figure 5. In both figures, the solid lines are from weighted nonlinear least-squares analysis of the data (Marquardt−Levenberg method[47]) according to eq VII. From literature values, it is possible to estimate the

parameters in eq VII. From Paper I (see Table 1), $k_2 = (4.2 \pm 0.2) \times 10^7$ $M^{-1}$ $s^{-1}$ and $k_g' = (1.80 \pm 0.03) \times 10^{10}$ $M^{-1}$ $s^{-1}$. Combining the values from Paper I, we obtain the ratio $(k_2/k_g')_I = (2.3 \pm 0.1) \times 10^{-3}$ M. From Table 1, $k_{10} = (2.0 \pm 0.3) \times 10^9$ $M^{-1}$ $s^{-1}$ and $k_5 = (7.8 \pm 0.8) \times 10^9$ $M^{-1}$ $s^{-1}$, giving an expected ratio of $(k_{10}/k_5)_{lit} = 0.27 \pm 0.05$.

From the value of $(k_{10}/k_5)_{lit}$, it appears to be a good approximation that the first factor in the denominator of eq VII is nearly equal to unity when $[Cl^-] = 0.2$ M and $[H_2O_2] = 5.345 \times 10^{-4}$ M. We adopted this assumption in fitting the data shown in Figure 4 and obtained $\Phi_{HO^\bullet} = 0.90 \pm 0.01$ and $(k_2/k_g')_{exp} = (5.75 \pm 0.26) \times 10^{-3}$ M.

This experimental value for $(k_2/k_g')_{exp}$ is 2.5 times as large as $(k_2/k_g')_I$, which is based on the results reported in Paper I.[26] The present experiments were carried out at a total ionic strength of ~0.2 M, whereas those in Paper I were carried out at ~0.01 M. All of the experiments in Paper I and in Figure 4 were carried out in the pH range $2 \le pH \le 5$. Under these conditions, $k_g' \approx k_3k_4/k_{-3}$ (see eq II). Reaction −3 is subject to a "negative salt effect", because it involves ions of opposite charge.[30] Anbar and Thomas observed a negative salt effect in their experiments on the rate of formation of $Cl_2^{-\bullet}$; that is, as the ionic strength increases, the formation rate of $Cl_2^{-\bullet}$, $k_g'$, decreases.[29]

According to the Debye−Hückel−Bronsted−Davies semi-empirical theory,[48] the ionic strength affects rate constants according to the following expression:

$$\log_{10}\frac{k_\mu}{k_0} = 2Z_1Z_2A\left\{\frac{\mu^{1/2}}{1+\mu^{1/2}}\right\} - b\mu \qquad \text{(VIII)}$$

where $k_\mu$ and $k_0$ are the rate constants at ionic strength $\mu$ and 0, respectively, $Z_1$ and $Z_2$ are the ionic charges, $A$ is the Debye−Hückel constant ($A = 0.509$ at 298 K), and $b$ is an empirical constant that is in the range ~0.2−0.3 for the few systems that have been studied in sufficient detail.[49] This equation explains the negative salt effect for reactions between ions of opposite charge.

According to eq VIII, the salt effect on the ratio $k_2/k_g'$ is given by the following expression:

$$\log_{10}[k_2/k_g']_\mu - \log_{10}[k_2/k_g']_0 = 2A\left\{\frac{\mu^{1/2}}{1+\mu^{1/2}}\right\} + b_r\mu \qquad \text{(IX)}$$

where $\mu$ is the ionic strength (expressed as moles/liter), $b_r = (b_3 - b_{-3} + b_4)$. Equation IX predicts that the ratio increases by a factor of between 1.7 and 4.0 (for $b_r = 0$ and for $b_r = 0.2$, respectively) when the ionic strength is increased from 0.01 to 0.2 M. The ratio of 2.5 found by comparing $(k_2/k_g')_{exp}$ with $(k_2/k_g')_I$ is generally consistent with these predictions, and corresponds to $b_r \approx 1$. If all of the salt effect is due to rate constant $k_g'$, then by using $k_2$ from Table 1 we obtain $k_g' = (0.73 \pm 0.10) \times 10^{10}$ $M^{-2}$ $s^{-1}$ at $\mu = 0.2$ M. This value is in good agreement with other reported values, as shown in Table 2.

The analysis of the data in Figure 5 is not straightforward for several reasons. Not only does the ratio $(k_2/k_g')$ depend on the salt effect and pH, but at low $[Cl^-]$, neglected reactions involving $Cl^\bullet$ (e.g., reaction 7) can deplete the observed $Cl_2^{-\bullet}$. At high enough $[Cl^-]$, this complication becomes negligible and scavenging becomes complete. In view of these complications, the least-squares analysis of the data in Figure 5 was carried out by simply using the experimental value for $(k_2/k_g')_{exp}$ obtained from Figure 4 in eq VII with $[H^+] = 0.1$ M. As a result, the fitted value of $\Phi_{HO^\bullet}$ should be meaningful, but the fitted value of $k_{10}/k_5$ has little real meaning. The least-squares analysis found $\Phi_{HO^\bullet} = 1.04 \pm 0.02$, and $(k_{10}/k_5)_{exp} = 0.82 \pm 0.09$. From the two values of $\Phi_{HO^\bullet}$ measured using the two independent sets of data at 248 nm (Figures 4 and 5), we obtain $\Phi_{HO^\bullet}$ (248 nm) $= 1.0 \pm 0.1$, where the uncertainty is $\pm\sigma$ (from propagation of errors).

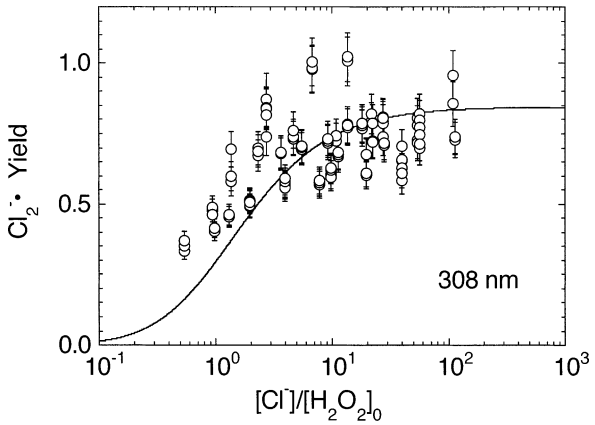


**Figure 6.** Dependence of $Cl_2^{-\bullet}$ yield (308 nm) on $[Cl^-]/[H_2O_2]$ at pH ~ 2. The solid line is nonlinear least-squares fit to eq VII.

At 308 nm, the absorption coefficient for $H_2O_2$ is only a few percent of that at 248 nm. Thus, higher concentrations of $H_2O_2$ were utilized in the experiments and the quality of the data was not as good as at 248 nm. The results obtained at 308 nm are plotted in Figure 6 as Yield vs $[Cl^-]/[H_2O_2]$ at pH = 2. In this case, the quantum yield $\Phi_{HO^\bullet}$(308 nm) is not very sensitive to the choice of the assumed rate constant ratio $k_2/k_g' = (5.75 \pm 0.26) \times 10^{-3}$ M (obtained from fitting the data in Figure 4). The result is $\Phi_{HO^\bullet}(308\text{ nm}) = 0.8 \pm 0.2$ ($\pm\sigma$, propagated errors), which is in good agreement with literature values and is not significantly different from unity.

**Numerical Simulations.** To determine whether the simplifications introduced in the data analysis are justified and to illustrate the nonlinear dependence of scavenging efficiency on some of the experimental variables, we carried out numerical simulations using all of the reactions (and rate constants) in Table 1, except for reaction 14, for which no solution-phase rate data are available. In addition, we included reactions 17 and 18 with $k_{17} = 1.0 \times 10^4$ $M^{-1}$ $s^{-1}$ [50] and $k_{18}$ and $k_{-18}$ from Jacob's review:[1]

$$ClOH^{-\bullet} + Cl^- \rightarrow HO^{-\bullet} + Cl_2^{-\bullet} \qquad (17)$$

$$H_2O \rightarrow HO^{-\bullet} + H^+ \qquad (18)$$

The scavenging efficiency can be expressed as the ratio $r = [Cl_2^{-\bullet}]_0/[HO^\bullet]_0$. The results of the simulations are presented in Figure 7 as a contour plot of the ratio as a function of pH and [NaCl]. The region corresponding to ≥98% scavenging efficiency is where the scavenger method is most accurate in determining hydroxyl yield. As pH decreases and [NaCl] increases, the scavenging efficiency increases. A cut parallel to the [NaCl] axis at pH = 1 corresponds to Figure 5, whereas a cut parallel to the pH axis at [NaCl] = 0.2 M corresponds to Figure 4. The simulations show good qualitative agreement with the experimental results, although they differ in detail, as reflected by the differences between the experimental rate constant ratios and those calculated from literature data. The differences are relatively minor and do not affect the measured quantum yields significantly.

**Discussion of Quantum Yields.** Previous measurements of $\Phi_D$ and $\Phi_{H_2O_2}$, and $\Phi_{HO^\bullet}$ are compiled in Tables 3 and 4,

**TABLE 2: Determinations of $k_g'$ at Room Temperature**

| $k_g'$, $\times 10^{-10}$ M$^{-2}$s$^{-1}$ | method | ratio | I, M | pH | ref |
|---|---|---|---|---|---|
| 1.16∼2.16 | PR | | < 0.15 | 1−3 | 1964[29] |
| 0.32∼1.84 | PR | | 1($NaClO_4$) | 0−3 | 1964[29] |
| 0.76 | $\gamma$-R | $k_g'/k_{thymine} = 1.9M^{-1}$ | < 0.2 | ∼1−3 | 1965[58] |
| 1.5 | PR | $k_g'/k_{thymine} = 3.75M^{-1}$ | < 0.2 | 0.8−3.4 | 1968[59] |
| 1.5 ± 0.12 | PR | | < 0.9 | 3 | 1973[30] |
| 1.85 or1.9 | PR | | 0.05/0.06 | 2 | 1973[60] |
| 1.81 ± 0.1 | FP | | ∼ 0.01 | 2 | 2002, Paper 1[26] |
| 0.73 ± 0.10[a] | FP | $k_2/k_g' = (5.75 \pm 0.26) \times 10^{-3}$ M | ∼ 0.2 | 2 | this work |

[a] At ionic strength = 0.2 M, if all of the salt effect is due to $k_g'$ (see text).

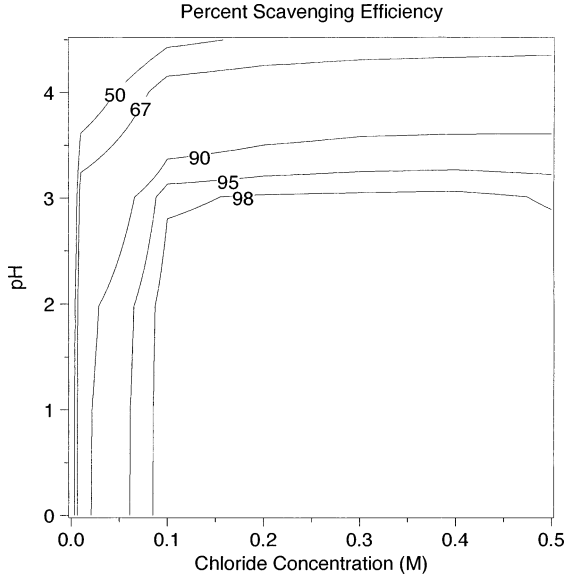


**Figure 7.** Scavenging efficiency (from numerical simulations) as a function of pH and [$Cl^-$] (see text for details).

**TABLE 3: Previous Measurements of the Quantum Yield of Hydrogen Peroxide Photodissociation ($\Phi_D$) or Loss ($\Phi_{H_2O_2}$) at Room Temperature**

| $\lambda$, nm | method[a] | $\Phi_D$ | $\Phi_{H_2O_2}$ | ref |
|---|---|---|---|---|
| 253.7 | HgLP | 1.39 ± 0.1[b] | | 1949[9] |
| 253.7 | UVLP | 1.7 ± 0.4[c] | | 1949[10] |
| 253.7 | UVLP | 0.98 ± 0.05 | | 1952[11] |
| 253.7 | HgLP | 1.9 ± 0.1 | | 1953[12] |
| 253.7 | UVLP | | 0.49 ± 0.07 | 1956[13] |
| 253.7 | UVLP | 1.00 ± 0.03[b] | | 1957[17] |
| 253.7 | UVLP | | 0.50[e] | 1957[17] |
| 253.7 | UVLP | 0.94 ± 0.06 | | 1959[14] |
| 253.7 | HgLP | 1.55 ± 0.16 | | 1991[18] |
| 253.7 | HgLP | 1.43 ± 0.15 | | 1991[18] |
| 313 | HgLP | 3−11[d] | | 1932[16] |
| 313 | UVLP | 1.7 ± 0.4[b] | | 1932[15] |

[a] HgLP = Hg lamp photolysis; UVLP = UV lamp photolysis; LFP = laser flash photolysis. [b] Averages of results obtained under various conditions. [c] Vapor phase. [d] 30 °C. [e] No error is reported.

respectively. The complexity in measuring $\Phi_D$, the total quantum yield for the destruction of hydrogen peroxide, is the variable chain length associated with the Haber−Weiss chain reactions.[31−33] The quantity usually desired is $\Phi_{H_2O_2}$, the primary quantum yield for photodissociation. Both Heidt[15] and Lea[9] found that $\Phi_D$ approaches a limiting value as the photolysis light intensity is reduced. Lea[9] found that $\Phi_D$ in the limit of low light intensity is independent of the concentration of hydrogen peroxide. Hunt and Taube[11] and Weeks and Matheson[13] qualitatively confirmed Lea's results and obtained limiting $\Phi_D$, which means that $\Phi_{H_2O_2}$ is ∼0.5, when the secondary reaction between hydrogen peroxide and the HO• radical is taken into account. In contrast, Dainton and Rowbottom[12] obtained $\Phi_D = 2$ and concluded that $\Phi_{H_2O_2}$ is near unity. Volman and Chen[14] measured $\Phi_D$ with and without allyl alcohol, a free radical scavenger. They assumed that $\Phi_D$ in allyl alcohol corresponds to $\Phi_{H_2O_2}$. In the absence and presence of allyl alcohol, the low-intensity limiting values for $\Phi_D$ were found to be 0.94 ± 0.06 and 0.54 ± 0.05, respectively. The latter value is thought to correspond to $\Phi_{H_2O_2}$. Because each $H_2O_2$ photodissociated produces two HO• radicals, $\Phi_{HO\bullet} = 2\Phi_{H_2O_2} = 1.08 \pm 0.1$ at 253.7 nm. Baxendale and Wilson[17] determined the quantum yield of hydrogen peroxide ($\Phi_D$) by 253.7 nm photolysis to be 1 at 25 °C. It was found that in the absence of air, formic acid, carbon monoxide, ethanol, and 2-propanol induce hydrogen peroxide decomposition which results in increased quantum yields as a function of light intensity. Using acetic acid to decrease the quantum yield until it reaches the lower limit when it is independent of acetic acid concentration, $\Phi_{H_2O_2} = 0.5$ at 25 °C was determined. Schäfer used 2-propanol to determine the quantum yield of hydrogen peroxide dissociation at 254 nm and followed the product acetone in the wavelength range of 250−310 nm.[18] Schäfer's experiment employed the same scavenger as Baxendale and Wilson,[17] who concluded that "2-propanol ($C_3H_8O$) induces the chain decomposition of hydrogen peroxide". Therefore, the higher values from Schäfer indeed are not $\Phi_{HO\bullet}$, but $\Phi_D$: $\Phi_D$=1.55 ± 0.16, 1.43 ± 0.15, and 1.22 ± 0.04. His results were also mistakenly identified as $\Phi_{HO\bullet}$ elsewhere.[51,52]

Direct measurements of $\Phi_{HO\bullet}$ are difficult because of the chain reactions and the difficulty of the detection of OH• in solution because of the relatively small absorption. Scavenger methods overcome both problems. The rapid scavenger reaction suppresses the Haber-Weiss chain reactions, and the scavenger reaction product is easier to detect because it absorbs light much more strongly than HO• radical. Hatada et al.[20] recently used *p*-nitrosodimethylaniline (RNO) as the scavenger to measure the quantum yield of hydroxyl radicals at 254 and 313 nm and

**TABLE 4: Scavenger Measurements of $\Phi_{HO\bullet}$ at Room Temperature**

| scavenger | photolysis $\lambda$, nm | method | monitored species | detection $\lambda$, nm | $\Phi_{HO\bullet}$ | year and ref |
|---|---|---|---|---|---|---|
| RNO | 254 | UVLP | RNO | 440 | 1.43 | 1974 [20] |
| RNO | 313 | UVLP | RNO | 440 | 1.43 | 1974 [20] |
| $SCN^-$ | 308 | LFP | $(SCN)_2^{-\bullet}$ | 475 | 0.98 ± 0.03 | 1990 [24] |
| $SCN^-$ | 351 | LFP | $(SCN)_2^{-\bullet}$ | 475 | 0.96 ± 0.04 | 1990 [24] |
| $Cl^-$ | 248 | LFP | $Cl_2^{-\bullet}$ | 364 | 1.0 ± 0.1 | this work |
| $Cl^-$ | 308 | LFP | $Cl_2^{-\bullet}$ | 364 | 0.8 ± 0.2 | this work |

obtained $\Phi_{HO\bullet} = 1.43$. Zellner et al.[24] used thiocyanate ions as the scavenger and obtained $\Phi_{HO\bullet} = 1$ at 308 and 351 nm in a laser flash photolysis experiment very similar to the present work.

From inspection of the results summarized in Table 4, it is clear that $\Phi_{HO\bullet} \approx 1$, independent of wavelength. The present results are in reasonable agreement with those obtained by Zellner et al.[24] but smaller than those of Hatada et al.[20] Note that Zellner et al. reported only the statistical precision of the measurements and did not discuss other sources of error.

Geminate recombination[53] in the solvent cage surrounding the $H_2O_2$ is probably responsible for the fact that $\Phi_{HO\bullet} < 2$. If every $H_2O_2$ dissociated and did not recombine after absorbing a photon, one would expect $\Phi_{HO\bullet} = 2$. When a $H_2O_2$ molecule absorbs a photon, the two energetic $HO^\bullet$ radical fragments find themselves on a strongly repulsive potential energy surface and hence recoil from one another. If they have sufficient energy and are oriented favorably with respect to each other and with respect to the solvent cage, they can escape from one another and diffuse separately in the solution. If they cannot escape from one another, the two free radicals recombine geminately, resulting in thermal heat release, but no net reaction. Based on the concept of geminate recombination, one would expect that photolysis at longer wavelengths would result in reduced values of $\Phi_{HO\bullet}$, but the results in Table 4 show no significant trend.

## Conclusions

A principle result of this work is that the quantum yield $\Phi_{HO\bullet} \approx 1$ in the aqueous phase at both 248 and 308 nm, in good agreement with previous work. The present work also shows that chloride ion is an efficient scavenger of hydroxyl radical and is a useful addition to the arsenal of methods that can be used to measure hydroxyl radical reaction rates. The scavenging efficiency depends on the chloride ion concentration and acidity, as expected. In addition, the results reveal a salt effect that is reasonably consistent with the Debye−Hückel-Bronstead-Davies empirical expression.

**Acknowledgment.** Financial support for this research was provided in part by the National Science Foundation (Atmospheric Chemistry Division). We also thank Robert Huie, Paul Wine, and Anthony Hynes for helpful discussions.

## References and Notes

(1) Jacob, D. J. *J. Geophys. Res.* **1986**, *91*, 9807.
(2) Graedel, T. E.; Weschler, C. J. *Rev. Geophys. Space Phys.* **1981**, *19*, 505.
(3) Anastasio, C.; Faust, B. C.; Allen, J. M. *J. Geophys. Res.* **1994**, *99*, 8231.
(4) Faust, B. C.; Anastasio, C.; Allen, J. M.; Arakaki, T. *Science* **1993**, *260*, 73.
(5) Zuo, Y.; Hoigné, J. *Environ. Sci. Technol.* **1992**, *26*, 1014.
(6) Zuo, Y.; Hoigné, J. *Science* **1993**, *260*, 71.
(7) Arakaki, T.; Faust, B. C. *J. Geophys. Res.* **1998**, *103*, 3487.
(8) Finlayson-Pitts, B. J.; Pitts, J. N., Jr. *Chemistry of the Upper and Lower Atmosphere*; Academic Press: San Diego, 2000.
(9) Lea, D. E. *Trans. Faraday Soc.* **1949**, *45*, 81.
(10) Volman, D. H. *J. Chem. Phys.* **1949**, *17*, 947.
(11) Hunt, J. P.; Taube, H. *J. Am. Chem. Soc.* **1952**, *74*, 5999.
(12) Dainton, F. S.; Rowbottom, J. *Trans. Faraday Soc.* **1953**, *49*, 1160.
(13) Weeks, J. L.; Matheson, M. S. *J. Am. Chem. Soc.* **1956**, *78*, 1273.
(14) Volman, D. H.; Chen, J. C. *J. Am. Chem. Soc.* **1959**, *81*, 1.
(15) Heidt, L. J. *J. Am. Chem. Soc.* **1932**, *54*, 2840.
(16) Qureshi, M.; Rahman, M. K. *J. Phys. Chem.* **1932**, *36*, 665.
(17) Baxendale, J. H.; Wilson, J. A. *Trans. Faraday Soc.* **1957**, *53*, 344.
(18) Schäfer, A. Photolyse von Nitrat, Bromat und H2O2 in wässrigen Lösungen: Bestimmung von Quantenausbeuten mit Hilfe von Radikalfängern, University Mainz, 1991.
(19) de Violet, P. F. *Rev. Chem. Intermed.* **1981**, *4*, 121.
(20) Hatada, M.; Kraljic, I.; Samahy, A. E.; Trumbore, C. N. *J. Phys. Chem.* **1974**, *78*, 888.
(21) Jablczynski, K.; Jablczyska, H. *Rocz. Chem.* **1930**, *10*, 579.
(22) Matheson, M. S.; Mulac, W. A.; Rabani, J. *J. Phys. Chem.* **1963**, *67*, 2613.
(23) Dogliotti, L.; Hayon, E. *TJPC* **1968**, *72*, 1800.
(24) Zellner, R.; Exner, M.; Herrmann, M. *J. Atmos. Chem.* **1990**, *10*, 411.
(25) Chin, M.; Wine, P. H. *J. Photochem. Photobio. A: Chem.* **1992**, *69*, 17.
(26) Yu, X.-Y.; Barker, J. R. *J. Phys. Chem. A* **2003**, *107*, 1313.
(27) Yu, X.-Y.; Bao, Z.-C.; Barker, J. R. *J. Phys. Chem. A.* **2003**, in preparation.
(28) Yu, X.-Y.; Barker, J. R. **2003**, in preparation.
(29) Anbar, M.; Thomas, J. K. *J. Phys. Chem.* **1964**, *68*, 3829.
(30) Jayson, G. G.; Parsons, B. J.; Swallow, A. J. *J. Chem. Soc., Faraday Trans. 1* **1973**, *69*, 1597.
(31) Haber, F.; Weiss, J. *Proc. R. Soc. London A.* **1934**, *147*, 332.
(32) Czapski, G.; Ilan, Y. A. *Photochem. & Photobiol.* **1978**, *28*, 651.
(33) Ferradini, C.; Foos, J.; Houee, C.; Pucheault, J. *Photochem. & Photobiol.* **1978**, *28*, 697.
(34) White, J. U. *J. Opt. Soc. Am.* **1942**, *32*, 285.
(35) Press, W. H.; Teukolsky, S. A.; Vetterling, W. T.; Flannery, B. P. *Numerical Recipes in FORTRAN. The Art of Scientific Computing*, 2 ed.; Cambridge University Press: Cambridge, 1992.
(36) Thomas, J. K.; Rabani, J.; Matheson, M. S.; Hart, E. J.; Gordon, S. *J. Phys. Chem.* **1966**, *70*, 2409.
(37) Hug, G. L. *Optical Spectra of Nonmetallic Inorganic Transient Species in Aqueous Solution*; U. S. Department of Commerce, National Bureau of Standards 1981; Vol. 69.
(38) Buxton, G. V.; McGowan, S.; Salmon, G. A.; Williams, J. E.; Wood, N. D. *Atmos. Environ.* **1996**, *30*, 2483.
(39) Treinin, A.; Hayon, E. *J. Am. Chem. Soc.* **1975**, *97*, 1716.
(40) Boltz, D. F.; Howell, J. A. *Colorimetric Determination of Nonmetals*, 1st ed.; New York Interscience: 1958.
(41) Yu, X.-Y. Kinetics of Free Radical Reactions Generated by Laser Flash Photolysis of $OH + Cl^-$ and $SO_4^- + Cl^-$ in the Aqueous Phase −− Chemical Mechanism, Kinetics Data and Their Implications. Ph. D. (Chemistry), The University of Michigan, Ann Arbor, MI, 2001.
(42) Raleigh, C. W. *Hydrogen Peroxide Physical Properties*; FMC Corporation: Pennsylvania, 1969.
(43) Taylor, R. C.; Cross, P. C. *J. Am. Chem. Soc.* **1949**, *71*, 2266.
(44) Nielson, S. O.; Michael, B. D.; Hart, E. J. *J. Phys. Chem.* **1976**, *80*, 2482.
(45) McElroy, W. J. *J. Phys. Chem.* **1990**, *94*, 2435.
(46) Bao, Z.-C.; Barker, J. R. *J. Phys. Chem.* **1996**, *100*, 9780.
(47) Synergy. KaleidaGraph; 3.51 ed.; Synergy Software, 2001.
(48) Perlmutter-Hayman, B. *Prog. React. Kinet.* **1971**, *6*, 239.
(49) Pankow, J. F. *Aquatic Chemistry Concepts*; Lewis Publishers Inc.: Chelsea, MI, 1991.
(50) Grigor'ev, A. E.; Makarov, I. E.; Pikaev, A. K. *High Energy Chem.* **1987**, *21*, 99.
(51) Buxton, G. V.; Salmon, G. A.; Barlow, S.; Malone, T. N.; McGowan, S.; Murray, S. A.; Williams, J. E.; Wood, N. D. Photochemical Sources and Reactions of Free Radicals in the Aqueous Phase. In *Heterogeneous and liquid-phase processes: laboratory studies related to aerosols and clouds*; Warneck, P., Ed.; Springer: Berlin, 1996; p 133.
(52) Warneck, P.; Mirabel, P.; Salmon, G. A.; Eldik, R. v.; Vinckier, C.; Wannowius, K. J.; Zetzsch, C. Review of the Activities and Achievements of the EUROTRAC Subproject HALIPP. In *Heterogeneous and liquid-phase processes: laboratory studies related to aerosols and clouds*; Warneck, P., Ed.; Springer: Berlin, 1996; p 7.
(53) Moore, J. W.; Pearson, R. G. *Kinetics and Mechanism*, 3rd ed.; John Wiley & Sons: New York, 1981.
(54) Weinstein, J.; Bielski, B. H. J. *J. Am. Chem. Soc.* **1979**, *101*, 58.
(55) Ross, A. B.; Neta, P. *Rate constants for reactions of inorganic radicals in aqeuous solution*; U. S. Department of Commerce, 1979; Vol. 65.
(56) Christenen, H.; Sehested, K. *J. Phys. Chem.* **1988**, *92*, 3007.
(57) Elliot, A. J.; Buxton, G. V. *J. Chem. Soc., Faraday Trans.* **1992**, *88*, 2465.
(58) Ward, J. F.; Myers, L. S., Jr. *Rad. Res.* **1965**, *26*, 483.
(59) Ward, J. F.; Kuo, I. "Steady state and pulse radiolysis of aqueous chloride solutions of nucleic acid components"; An international conference sponsored by Argonne National Laboratory: Argonne National Laboratory: Argonne, IL, 1968.
(60) Ogura, H.; Hamill, W. H. *J. Phys. Chem.* **1973**, *77*, 2952.